J Mater Sci: Mater Electron (2015) 26:162–167
DOI 10.1007/s10854-014-2378-0

Low temperature sintering properties of LiF-doped $BaTiO_3$-based dielectric ceramics for AC MLCCs

Min-Jia Wang · Hui Yang · Qi-Long Zhang · Dan Yu · Liang Hu · Zhi-Sheng Lin · Zi-Shan Zhang

Received: 8 July 2014 / Accepted: 7 October 2014 / Published online: 1 November 2014

Abstract The effects of LiF addition on phase evolution, microstructure and dielectric properties of $BaTiO_3$ based ceramics were investigated. The LiF addition lowered the sintering temperature of $BaTiO_3$ based ceramics effectively from 1,380 to 1,100 °C. Orthorhombic-to-pseudocubic phase transition appeared as increasing sintering temperature or LiF content. Li^+ dissolved in the lattice of $BaTiO_3$, replaced Ti^{4+} site, produced oxygen vacancies and further inhibited the grain growth. F^- entered into O^{2-} site, might cause weakening of oxygen bond strength, together with the low-melting-point liquid phase sintering of LiF, facilitated the formation of uniform dense and fine-grained structure and maintained good dielectric properties. Samples with 2 wt% LiF sintered at 1,100 °C showed excellent dielectric properties: $\varepsilon_r = 1{,}956$, $\tan\delta = 0.8$ % (at 1 kHz), $\Delta C/C_{25} < 10.44$ % (−55–125 °C) and alternating current breakdown voltage $E > 4.50$ kV/mm.

1 Introduction

$BaTiO_3$-based ceramics have been used as a dielectric material in many fields: electronic information, automatic control, biological technology, energy management and traffic control component, in which it must be modified chemically and physically to meet the requirements of various dielectric applications. The AC MLCCs production is mainly applied in the power supply bypass and decoupling, especially in the strong alternating electric field, which requires high capacitance but can tolerate moderate loss, temperature dependence, and voltage dependence of capacitance [1–4]. So the dielectric will not break down easily, in spite of the accumulation of heat caused by electrostrictive telescopic and inner electric field stress. Currently, considerable studies have illustrated that rare earth elements such as Y, Nd and La can successfully modify dielectric properties of $BaTiO_3$-based ceramics [5–7]. Our recent research has found that Y/Mg/Ga/Si co-doped $BaTiO_3$ ceramics possessed excellent dielectric properties: $\varepsilon_r = 2{,}487$, $\tan\delta = 0.7$ %, $\Delta C/C_{25} < 6.56$ % and AC breakdown voltage $E \sim 4.02$ kV/mm. It indicated that Y^{3+} dissolved in the lattice of $BaTiO_3$, replacing Ba^{2+} site and Ti^{4+} site, while Mg^{2+} replaced Ti^{4+} site. The replacing process inhibited grain growth, caused a phase transition from tetragonal to pseudocubic, reduced the dielectric loss, and flattened the temperature dependence of capacitance curve (TCC). The incorporation of Ga^{3+} could improve sintering behavior and increase permittivity. Also, SiO_2 was one of most effective additives for improving the sintering and dielectric properties of $BaTiO_3$ ceramics [8]. However, similar to the other single-doped or double-doped rare earth $BaTiO_3$ ceramics [9–11], the sintering temperature of Y/Mg/Ga/Si co-doped $BaTiO_3$ ceramics is higher than 1,300 °C, which restricts the real application. Many researchers have already investigated the low temperature sintering of these ceramics such as using well monodispersed nanopowders synthesized by a wet-chemical routine as raw materials or adding low-melting-point sintering aids into the dielectric ceramics and so on [12–15], Among them, adding sintering aids is the most effective and convenient method to decrease the sintering temperature.

M.-J. Wang · H. Yang · Q.-L. Zhang (✉) · D. Yu · L. Hu
Department of Materials Science and Engineering, Zhejiang University, Hangzhou 310027, China
e-mail: mse237@zju.edu.cn

Z.-S. Lin · Z.-S. Zhang
Fujian Torch Electron Technology Co., LTD., Quanzhou 362000, China

Previous studies illustrated that LiF is a very effective sintering aid for electronic ceramics such as MgO, $(Mg_{0.95}Zn_{0.05})_2(Ti_{0.8}Sn_{0.2})O_4$ and other perovskites [16–19]. LiF has a face centered cubic rock salt structure which is similar with that of $BaTiO_3$ and a low melting point of 845 °C. In the paper, the key purpose is to decrease the sintering temperature of Y/Mg/Ga/Si co-doped $BaTiO_3$ ceramics via LiF addition, and to prepare a kind of AC $BaTiO_3$ ceramics with low dielectric loss and high capacitance temperature stability.

2 Experimental

The starting material was high purity commercial grade $BaTiO_3$ powder (Ba/Ti = 0.999), which was synthesized hydrothermally with particle size of ~ 0.5 μm. Doped additives Y_2O_3 (99.99 %), MgO (99 %), Ga_2O_3 (99.99 %), and SiO_2 (AR) were weighed in a proper proportion. They were mixed together with above $BaTiO_3$ powder and 1–3 wt% LiF (AR). The mixed powders were ball-milled in ethanol for 6 h using zirconia balls of 2 mm in diameter. After being dried and sieved, 8 wt% polyvinyl alcohol (PVA) was added as binder. The slurry was granulated and made into cylindrical compacts about 10 mm in diameter and 1 mm in thickness under a uniaxial pressure of 300 MPa. Then the compacts were baked at 500 °C for 1 h to eliminate the binder, and sintered in air between 1,060 and 1,220 °C at a rate of 3 °C/min.

The crystalline phase of the sintered samples was characterized by X-ray diffraction (XRD, EMPYREAN, PAN Analytical Co., Netherlands, Cu-Kα) in the 2θ range 10°–80° with a step of 0.01° after ground the compacts into powders. The bulk density of the sintered samples was measured using Archimedes method. The fracture surface of sintered samples was determined using a scanning electron microscope (FSEM, SIRION-100, and FEI, USA). TEM samples were prepared by mechanical polishing and ion beam thinning (Gatan PIPS), and then observed by transmission electron microscopy (TEM, JEM-1200EX, JEOL). Energy dispersive spectroscopy (EDS) was used to analyze the composition profiles of the dopants in the core–shell structure.

Silver paste electrodes were fired at 650 °C for 30 min on both surfaces of the samples. The permittivity and dielectric loss of the samples were measured in a range from −55 to 125 °C using an HP 4278 LCR meter at 1 kHz with 1Vrms. The AC breakdown voltage (BDV) was determined by an AC voltage tester 7120 at 50 Hz with a rate of 200 V/s (Maximum 5 kV).

3 Results and discussion

The XRD patterns of the samples by addition of 0–3 wt% LiF sintered at different temperatures for 3 h are shown in Fig. 1. All these samples exhibit a pure perovskite structure without any trace of impurity phase. The sample with 0 wt% LiF, 3 wt% LiF sintered at 1,100 °C, and 2 wt% LiF sintered at 1,220 °C show the pseudocubic structure, while the other samples show orthorhombic structures, which can be clearly observed through the enlarged view of (022) and (200) peak at diffraction angle (2θ) 44°–46°. The relative ratio change in the peak intensity of the (200) plane to that of the (022) plane indicates the orthorhombic-to-pseudocubic phase transition and decrease in the orthogonality with the increase of LiF content and temperature. In addition, the (110) peak of the sample with 3 wt% LiF shifts to higher 2θ degrees compared with undoped sample, which is attributed to the lattice distortion resulted from the incorporation of Li^+ and F^-. On one hand, Li^+ replaces Ti^{4+} site as an acceptor, and produces large amounts of oxygen vacancies, which can be explained by the electroneutrality equation: $LiF \leftrightarrow Li_{Ti}''' + V_O{\cdot\cdot} + F_O{\cdot}$, according to Krőger-Vink notation. Although the ionic radius of Li^+ (0.76 Å) is larger than Ti^{4+} (0.605 Å), numerous oxygen vacancies caused by the balance of valence have more critical contribution. On the other hand, F^- replaces O^{2-} site. F^- ionic radius (1.33 Å) is smaller than O^{2-}(1.40 Å) [20]. So the volume of unit cell decreases, and the (110) peak moves to higher angles. It can be seen from Fig. 1b that for the sample with 2 wt% LiF, the (111) peak of orthorhombic structure shifts to lower 2θ degrees with increasing the sintering temperature from 1,060 to 1,180 °C. This result indicates that LiF can dissolve into the lattice of $BaTiO_3$.

Bulk densities-temperatures curves of the samples differ in the amount of LiF addition are illustrated in Fig. 2. The sample with 2 wt% LiF addition shows the highest densities among the whole sintering temperatures. Densification temperature also varies with the changes of LiF content, and it can also be reflected from SEM images of the sample fracture surface in Fig. 3. It can be seen that the sample with 2 wt% LiF sintered at 1,060 °C shows disorder grain distribution. High-uniformity micromorphology of grains with reasonably good close packing was obtained at 1,100 °C. However, porous microstructure occurred due to the orthorhombic-to-pseudocubic phase transition (shown in Fig. 1b) as the temperature increases from 1,100 to 1,180 °C. Further increasing temperature to 1,220 °C, no orthorhombic-to-pseudocubic phase transition happened, dense structure was obtained again, but abnormal grain growth occurred. As shown in Fig. 3h, the morphology with large grain size (~5 μm) and small liquid phase were observed in the sample with 3 wt% LiF sintered at 1,140 °C. Thus, we can conclude that the content of LiF dissolved in the lattice of $BaTiO_3$ is lower 3 wt%. Based on the above phenomenon, a plausible explanation is proposed here. The addition of LiF as sintering aid in the $BaTiO_3$

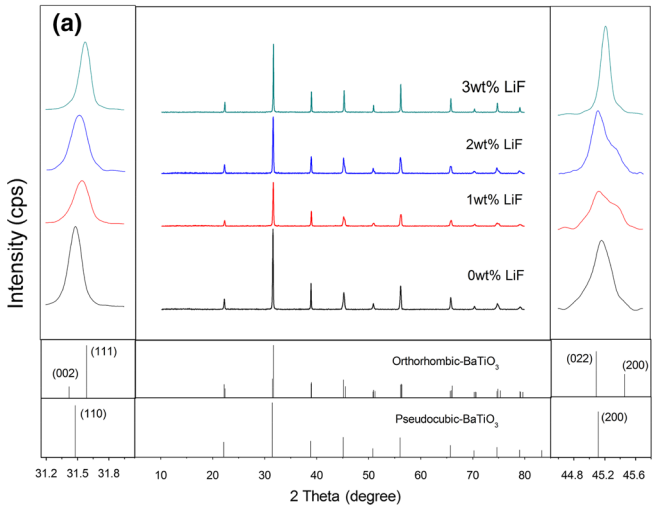

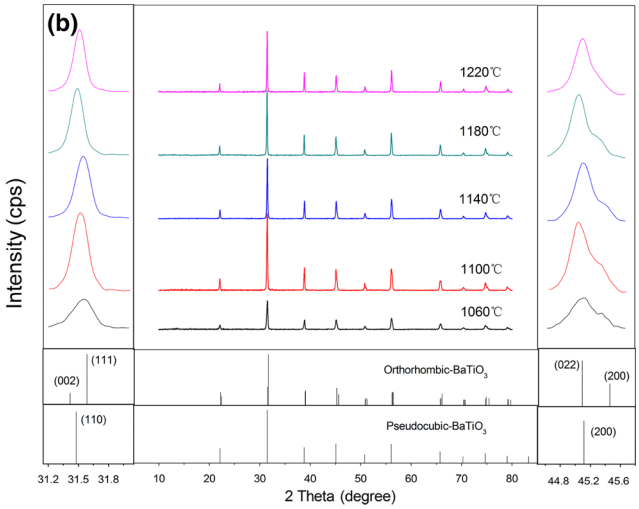

Fig. 1 X-ray diffraction patterns of **a** the samples with different amount of LiF sintered at 1,100 °C (*line* profiles of (110), (111), (002), (022) and (200) peaks shown in the *inset*); **b** samples with 2 wt% LiF content sintered at various temperatures (*line* profiles of (110), (111), (002), (022) and (200) peaks shown in the *inset*)

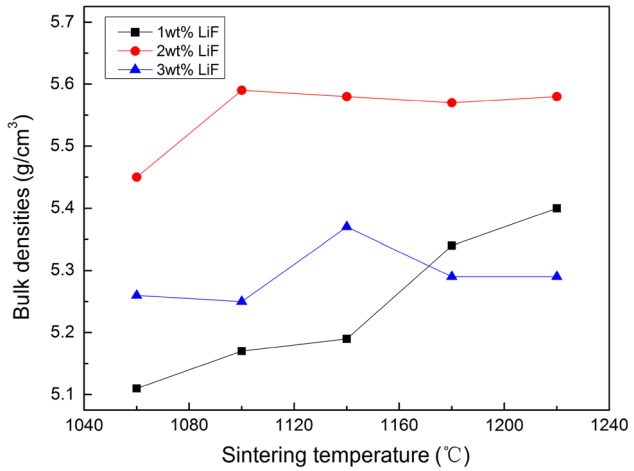

Fig. 2 Bulk densities-temperatures curves of the samples with 1–3 wt% LiF content

ceramics can bring about two effects during the sintering process: On one hand, with a small amount of Li^+ and F^- entering into the lattice, the substitution of smaller F^- for O^{2-} will cause weakening of oxygen bond strength. At the same time, the oxygen vacancies produced by the replacement of Li^+ for Ti^{4+} will facilitate the diffusion process, promote the ion migration, benefit the sintering densification and further decreases intrinsic sintering temperature. The above mechanism of Li^+ is similar to that of Cu^{2+} [21]. On the other hand, since the LiF has a low melting point of 845 °C, liquid phase is formed during the sintering which enhances grain boundary mass transport significantly [22]. TEM investigation is carried out on the sample with 2 wt% LiF content sintered at 1,100 °C, and Fig. 4 shows the bright field image of the core–shell structure and the results of EDS line profile analysis. It indicates that Y and Ga distribute non-homogeneously in core and shell, while Mg, Si and F are uniformly distributed across the shell-to-core boundary. MgO-Y_2O_3-based $BaTiO_3$ is reported that can form the core–shell structure [23, 24], and the formation mechanism is accepted to be inter-lattice diffusion [25, 26]. LiF is also helpful for the formation of core–shell structure, and the mechanism that solution reprecipitation with limited grain growth at low temperatures is proposed [27].

Dielectric properties of the samples with 1–3 wt% LiF sintered at various temperatures are listed in Table 1. The room temperature permittivity of all the samples with LiF is smaller than the one without LiF, which is attributed to the decrease in ionic polariability of the dipole moment caused by the substitution of Li^+ and F^-. The values of α (Li^+) and α (F^-) are 1.20 and 1.62 $Å^3$, respectively, smaller than α (Ti^{4+}) (2.94 $Å^3$) and α (O^{2-}) (2.00 $Å^3$) [28]. According to the Clausius–Mossotti equation, the permittivity of ceramics is also determined by the dipoles in unit cell volume [29], so higher density means there are more dipoles in a unit cell volume, and hence the permittivity of the sample sintered at 1,100 °C is larger than that sintered at 1,060 °C. When the temperature is higher than 1,100 °C, orthorhombic-to-pseudocubic phase transition makes the permittivity continue to increase. The sample without LiF sintered at 1,380 °C exhibits lowest dielectric loss properties due to domain-wall pinning resulted from orientation of the electric and elastic dipoles caused by the incorporation of Mg [30]. It shows obvious deterioration in the dielectric loss of the sample with 1 wt% LiF sintered at 1,220 °C due to inhomogeneous distribution of crystal

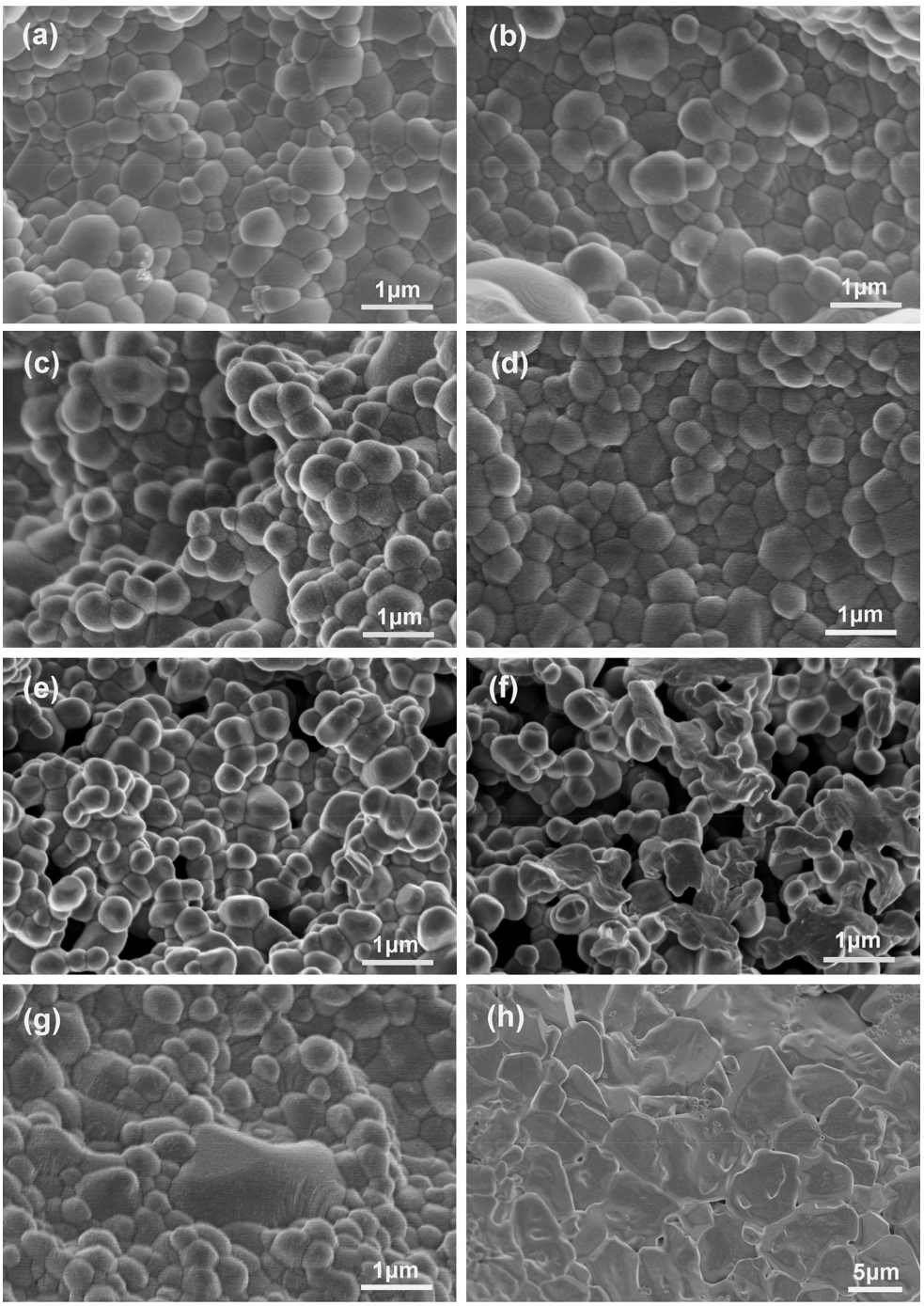

Fig. 3 SEM of the fracture surfaces of $BaTiO_3$ samples: **a** the sample without LiF sintered at 1,380 °C, **b** the sample with 1 wt% LiF sintered at 1,220 °C, **c** the sample with 2 wt% LiF sintered at 1,060 °C, **d** the sample with 2 wt% LiF sintered at 1,100 °C, **e** the sample with 2 wt% LiF sintered at 1,140 °C, **f** the sample with 2 wt% LiF sintered at 1,180 °C, **g** the sample with 2 wt% LiF sintered at 1,220 °C, **h** the sample with 3 wt% LiF sintered at 1,140 °C

grains. However, appropriate LiF content can keep dissipation in a relative low stable value due to the formation of uniform microstructures with narrow grain size distribution and less defects. Figure 5 shows temperature coefficient of capacitance (TCC) curves of the samples with 0–3 wt% LiF sintered at various temperatures for 3 h. The sample with 2 wt% LiF content sintered at 1,100 °C displays the best capacitance-temperature stability among all the samples with LiF addition, which is associated with the core–shell structure and the volume fraction occupied by core and shell respectively [31]. Excessive and insufficient addition of LiF will deteriorate the TCC, maybe due to the

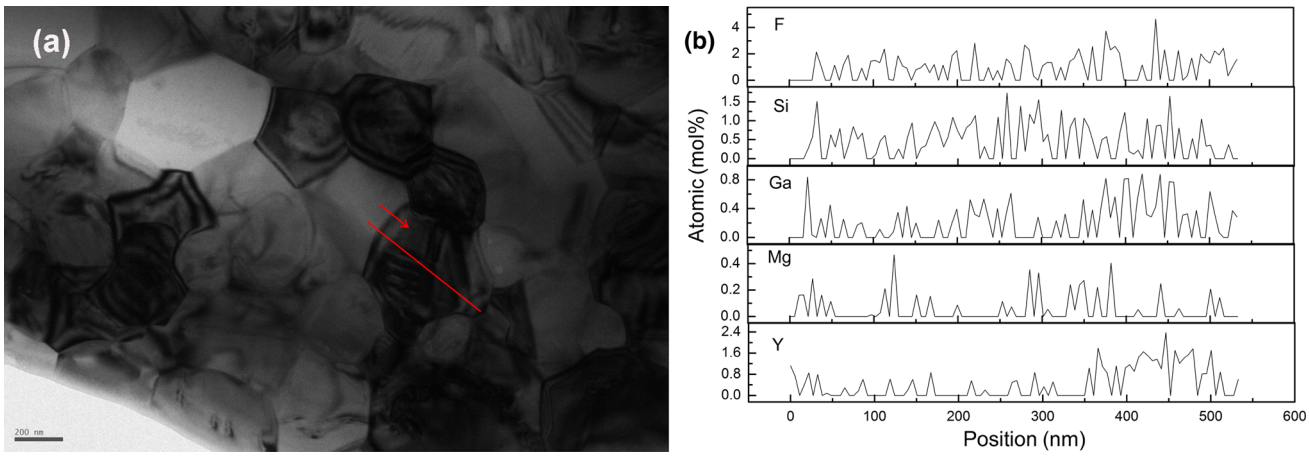

Fig. 4 TEM bright field image of the sample with 2 wt% LiF sintered at 1,100 °C and EDS *line* profile for a typical core–shell grain of five dopants

Table 1 Dielectric properties of samples with 1–3 wt% LiF sintered at various temperatures

Specimen	Permittivity	Dielectric loss	Max|$\Delta C/C_{25}$| (%)	AC BDV (kv/mm)
1 wt% LiF 1,220 °C	2,331	0.019	15.04	>4.07
2 wt% LiF 1060 °C	1,647	0.009	10.87	>4.21
2 wt% LiF 1,100 °C	1,956	0.008	10.44	>4.50
2 wt% LiF 1140 °C	2,101	0.009	11.93	>4.39
2 wt% LiF 1,180 °C	2,274	0.010	16.40	>4.40
2 wt% LiF 1,220 °C	2,401	0.011	17.59	>4.17
3 wt% LiF 1,140 °C	2,304	0.010	54.93	>4.13

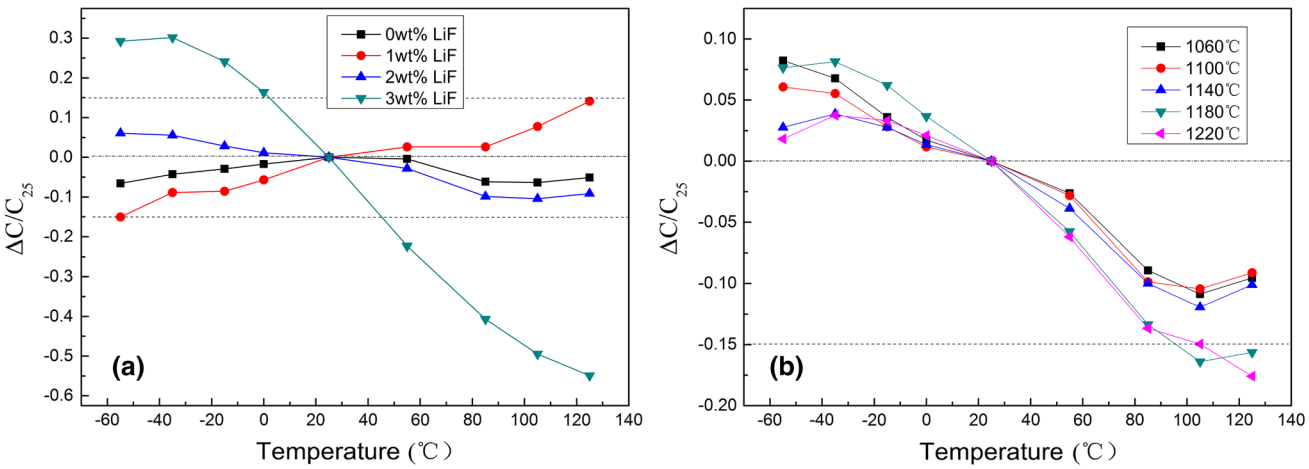

Fig. 5 Temperature coefficient of capacitance $(C\text{-}C_{25})/C_{25}$ of the sample **a** with 0–3 wt% LiF sintered at each own optimal temperature; **b** with 2 wt% LiF sintered at various temperatures for 3 h

excessive liquid phase and incompletely sintering. The AC voltage resistance is a crucial parameter for AC MLCCs. The dielectric breakdown phenomenon of dielectrics is structure-sensitive, and breakdown strength values may scatter widely according to the characteristics of the microstructure and thickness of dielectric materials [32]. Besides, the breakdown field strength can also be influenced by the doped elements, the dopants concentration, sintering temperature and the soaking time [33]. The addition of LiF can significantly improve the AC voltage

resistance characteristics on the basis of the $BaTiO_3$–Y_2O_3–MgO–Ga_2O_3–SiO_2 system. It is known that the presence of some defects such as grain boundary, phase boundary and lattice imperfection can limit the movement of charged ions. The addition of LiF brings about liquid phase and more lattice distortion, leads to the generation of more helpful defects, and increases the AC breakdown voltage.

4 Conclusions

In the paper, the influence of LiF-containing additives on the dielectric properties and microstructures of $BaTiO_3$–Y_2O_3–MgO-Ga_2O_3-SiO_2 was investigated. Li^+ and F^- can enter into the lattice. Li^+ replaces Ti^{4+} site, produces massive oxygen vacancies and further inhibits the grain growth. F^- replaces O^{2-} site, causes weakening of oxygen bond strength, thus reduces the intrinsic sintering temperature and facilitates the diffusion process. Meanwhile, LiF is a low melting point (845 °C) material, so liquid phase is formed during the sintering which enhances grain boundary mass transport significantly. An addition of 2 wt% LiF to the doping $BaTiO_3$ can increase the AC breakdown voltage due to the helpful defects that limit the movement of charged ions. Dielectric properties: $\varepsilon_r = \sim 1{,}956$, $\tan\delta = \sim 0.8$ % (at 1 kHz), $\Delta C/C_{25} < \sim 10.44$ % (from −55 to 125 °C) and AC breakdown voltage $E > \sim 4.50$ kV/mm can be achieved in the $BaTiO_3$-2 mol% Y_2O_3-3 mol% MgO-1 mol% Ga_2O_3-0.5 mol% SiO_2 -2 wt% LiF ceramics sintered at 1,100 °C. The ceramics sintered at low temperatures with excellent dielectric properties turns out to be promising for AC multilayer ceramic capacitors.

Acknowledgments The authors gratefully acknowledge the financial support from the National High Technology Research and Development Program of China (863 Program) (No. 2013AA030701).

References

1. M. Kong, S.L. Jiang, T.T. Xie, H.B. Zhang, Microelectron. Eng. **86**, 2320–2323 (2009)
2. X. Ning, P.Y. Ping, W. Zhuo, J. Am. Ceram. Soc. **95**, 999–1003 (2012)
3. M.J. Pan, C.A. Randall, IEEE Electr. Insul. M **26**, 44–50 (2010)
4. R.B. Amin, H.U. Anderson, C.E. Hodgkins, U.S. Patent, (1978) 4,082,906
5. S. Singh, P. Singh, O. Parkash, D. Kumar, J. Alloy, Compd. **493**, 522–528 (2010)
6. W.X. Zhang, L.X. Cao, G. Su, W. Liu, J. Mater. Sci-Mater. El. **24**, 1801–1806 (2013)
7. C. Behera, R.N.P. Choudhary, P.R. Das, J. Mater. Sci-Mater. El. **25**, 2086–2095 (2014)
8. M.J. Wang, H. Yang, Q.L. Zhang, Z.S. Lin, Z.S. Zhang, D. Yu, L. Hu, Mater. Res. Bull. **60**, 485–491 (2014)
9. W.H. Lee, C.Y. Su, J. Am. Ceram. Soc. **90**, 3345–3348 (2007)
10. A.P.A. Moraes, A.G. Souza, P.T.C. Freire, J. Mendes, J.C. M'Peko, A.C. Hernandes, E. Antonelli, M.W. Blair, R.E. Muenchausen, L.G. Jacobsohn, W. Paraguassu, J. Appl. Phys. **109**, 124102 (2011)
11. S.L. Leng, G.R. Li, L.Y. Zheng, W. Shi, Y. Zhu, J. Mater. Sci-Mater. El. **24**, 431–435 (2013)
12. Q.L. Zhang, F. Wu, H. Yang, D. Zou, J. Mater. Chem. **18**, 5339–5343 (2008)
13. I. Burn, J. Mater. Sci. **17**, 1398–1408 (1982)
14. M. Valant, D. Suvorov, R.C. Pullar, K. Sarma, N.M. Alford, J. Eur. Ceram. Soc. **26**, 2777–2783 (2006)
15. X.F. Su, M. Tomozawa, J.K. Nelson, D.B. Chrisey, J. Mater. Sci-Mater. El. **24**, 2135–2140 (2013)
16. A. Kan, H. Ogawa, T. Moriyama, J. Mater. Res. **27**, 915–920 (2012)
17. C.L. Tsai, M. Kopczyk, R.J. Smith, V.H. Schmidt, Solid State Ionics **181**, 1083–1090 (2010)
18. G.G. Yao, P. Liu, Ceram. Int. **38**, 2239–2242 (2012)
19. S. Marinel, M. Pollet, G. Allainmat, J. Mater. Sci. **38**, 4027–4032 (2003)
20. J.J. Bian, J.Y. Wu, L. Wang, J. Eur. Ceram. Soc. **32**, 1251–1259 (2012)
21. W. Jo, J.B. Ollagnier, J.L. Park, E.M. Anton, O.J. Kwon, C. Park, H.H. Seo, J.S. Lee, E. Erdemd, R.A. Eichel, J. Rödel, J. Eur. Ceram. Soc. **31**, 2107–2117 (2011)
22. Y.Z. Hao, H. Yang, G.H. Chen, Q.L. Zhang, J. Alloy. Compd. **552**, 173–179 (2013)
23. S.C. Jeon, C.S. Lee, S.J.L. Kang, J. Am. Ceram. Soc. **95**, 2435–2438 (2012)
24. C.Y. Chang, W.N. Wang, C.Y. Huang, J. Am. Ceram. Soc. **96**, 2570–2576 (2013)
25. H. Kishi, Y. Okino, M. Honda, Y. Iguchi, M. Imaeda, Y. Takahashi, H. Ohsato, T. Okuda, Jpn. J. Appl. Phys. **36**, 5954–5957 (1997)
26. T. Wang, X.H. Wang, H. Wen, L.T. Li, Int. J. Miner. Metall. Mater. **16**, 345–348 (2009)
27. S.F. Wang, T.C.K. Yang, W. Huebner, J.P. Chu, J. Mater. Res. **15**, 407–415 (2000)
28. R.D. Shannon, J. Appl. Phys. **73**, 348–366 (1993)
29. M.T. Sebastian, Dielectric Materials for Wireless Communication, Elsevier, 2008
30. B. Su, T.W. Button, J. Appl. Phys. **95**, 1382–1385 (2004)
31. Y. Park, Y.H. Kim, H.G. Kim, Mat. Lett. **28**, 101–106 (1996)
32. H. Naghib-zadeh, C. Glitzky, I. Dörfel, T. Rabe, J. Eur. Ceram. Soc. **30**, 81–86 (2010)
33. G.H. Maher, J.M. Wilson, S.G. Maher, Carts-conference, USA, (2006)